Twenty-Fifth Symposium (International) on Combustion/The Combustion Institute, 1994/pp. 1167–1173

# RAMAN MEASUREMENTS AND JOINT PDF MODELING OF A NONPREMIXED BLUFF-BODY-STABILIZED METHANE FLAME

SANJAY M. CORREA AND ANIL GULATI
*General Electric Research Center*
*Schenectady, NY 12301, USA*

AND

STEPHEN B. POPE
*Cornell University*
*Ithaca, NY 14853, USA*

Mixture fraction, temperature, and major species in a recirculation-stabilized nonpremixed methane-air flame are (1) measured using laser Raman scattering and (2) calculated using the joint velocity-composition probability density function (PDF) model, appropriately combined with an elliptic mean flow solver. The Raman system was modified to account for the significant levels of laser-induced fluorescence (LIF) and incandescence encountered in the rich sooty zone of the flame. The joint PDF contains three velocity components, which are modeled by Langevin equations, and five thermochemical scalar variables with mixing given by linear deterministic relaxation to the mean and chemistry by a four-step steady-state reduced scheme. The flame is characterized by significant finite-rate chemistry, including, unlike a $CO/H_2/N_2$ fuel in the same apparatus, strong bimodality in the temperature-mixture fraction scatter plots. Calculations are compared with Raman data on temperature and major species. The agreement is in general reasonable, with the largest discrepancies being caused by the breakdown of the assumption of a chemical steady state for the cool fuel-rich gas at the core of the flame. Large discrepancies are found on the peak CO, as in other similar studies, confirming a need for better measurements of CO than Raman spectroscopy can provide. The model overpredicts the degree of extinction. The radial flux of the mixture fraction calculated directly from the joint PDF is compared with the flux given by an *a posteriori* gradient diffusion calculation, indicating no (radial) counter-gradient diffusion and a "turbulent Schmidt number" of about 0.4.

## Introduction

Chemical kinetics and their interactions with turbulence control combustion phenomena such as emissions and the related issue of flame stability, which have become significant technology drivers [1,2]. The pressure-corrected mean Navier–Stokes/*assumed-shape* PDF/$k$-$\varepsilon$ turbulence model does not account rigorously for the turbulence-chemistry aspects of these issues, but affords significant geometric flexibility and rapid convergence for pressure-dominated internal flow [3]. On the other hand, the joint (velocity-composition) probability density function (PDF) transport model includes turbulence and chemistry with single-point closure [4]. The PDF model has been widely used to compute turbulent *jet* flames, both in the composition-only form [5] and in the joint velocity-composition form [6–8]. More recently, the joint PDF model has been extended to "elliptic" (recirculating) flow and applied to the computation of $CO/H_2$ bluff-body flames [9], marking a step toward the recirculation-stabilized flow fields found in practical burners. Bluff bodies also eliminate the pilot stabilization necessary in jet flames at high Reynolds numbers.

There are other approaches, intermediate in complexity and cost, between the assumed-shape PDF model (No. 1) and the joint velocity-composition PDF transport model (No. 4). The "conditional moment closure" model (No. 2) solves conventional time-averaged field equations for the means of reactive scalars conditioned on the mixture fraction [10] and is applicable only when fluctuations about this conditional mean are small. The scalar PDF model (No. 3) does not treat the velocity part of the PDF, using instead conventional turbulence modeling to supply the scalar (and momentum) fluxes [11]. Arguments of computational cost are usually made to support model numbers 1 through 3; however, the speedup achieved in parallelizing particle tracking PDF computations shows that they can be usable in practical design codes [12].

Methane is of particular interest in this context for scientific reasons, because it affords strong finite-rate

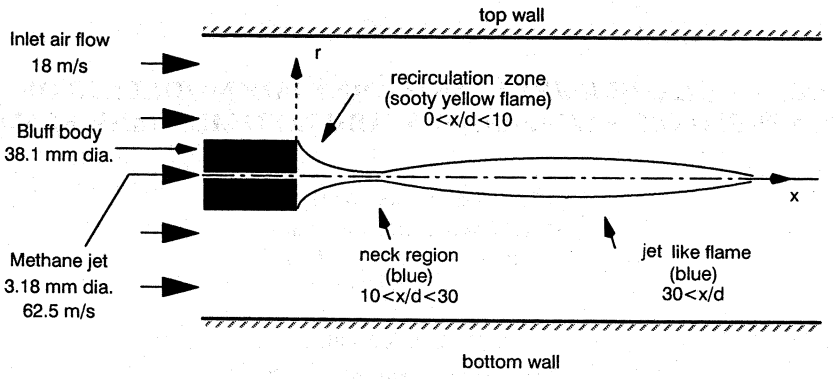


FIG. 1. Non-premixed bluff-body-stabilized methane flame; $d$ is the jet diameter.

chemistry effects and well-studied reduced kinetic schemes, and for practical reasons, because there is a significant worldwide natural-gas economy. For example, about 50 GW of new gas-fired power plants are being sold annually. The development and qualification of predictive tools—with the required geometry, chemistry, and turbulence capabilities—will aid this industry.

Of the many prior bluff-body flame studies, the most closely related is that of Masri et al. [13] who also used fluorescence-corrected Raman spectroscopy of methane-air flames. The present work uses a jet that is twice as big and stresses the jet-dominated regime, which is less susceptible to large-scale shedding off the bluff body; greater degrees of extinction are found. Hence, the new contributions of this paper are Raman temperature and major species measurements in the jet-dominated regime of a bluff body–stabilized nonpremixed methane-air flame, and comparisons with predictions of the joint PDF/elliptic mean flow computational fluid dynamics (CFD) model.

## Experimental Setup and the Raman Measurement Technique

The bluff-body burner and the inflow conditions are shown in Fig. 1. The axisymmetric bluff body has an outer diameter of 38.1 mm with an axial jet of 3.18-mm diameter "$d$" located in the center. It is well known that parts of this flow field—notably, the annular shear layer shed off the bluff body—can be dominated by unsteady effects. Care was taken to operate in a velocity (jet and coflow) regime where the flame was steady. The cold jet Reynolds number is 12,000, based on the jet diameter and jet exit velocity of 62.5 m/s. The coflow air velocity is 18 m/s. The back surface of the bluff body is coated with a thermal barrier material to reduce heat loss. The flame is stabilized by the recirculation zone provided by the bluff body. The tunnel cross section is 15 × 15 cm, large enough not to interfere with the flame. (The calculations are made for a circular duct of the same cross-sectional area.) Visual observations of methane flames at various air and fuel-jet velocities were used to select the conditions for the Raman-scattering measurements reported below. This flame is anchored by the bluff body and is almost extinguished in the neck region, before reigniting further downstream.

The Raman system is based on a flashlamp-pumped dye laser that provides pulses of ≈1 J in 2–4 $\mu$s, within a 0.2-nm bandpass at 488 nm at a repetition rate of 10 Hz. The light scattered at right angles is collected by two lenses, separated in frequency by a 0.75-m-spectrometer, and is detected by eight photomultiplier tubes (PMTs). The PMTs detect anti-Stokes vibrational Raman scattering from $N_2$, Stokes vibrational Raman scattering from $N_2$, $O_2$, $H_2$, $H_2O$, CO, and $CO_2$, and Rayleigh scattering. The temporal resolution (2–4 $\mu$s) of the technique is limited by the laser pulse length, the spatial resolution (0.2 × 0.2 × 0.6 mm) is limited by the spectrometer entrance slit and the collection optics, and the data acquisition rate is limited by the laser repetition rate. The flame luminescence was broadbanded throughout the visible region and was reduced by a polarization filter in the collection optics. The polarization vector was aligned to pass horizontally polarized Raman- and Rayleigh-scattered light.

The instantaneous temperature on every laser shot was determined in three independent ways: (1) the Stokes-anti-Stokes (SAS) ratio from nitrogen, which yields the temperature directly [14]; (2) an iterative scheme in which an initial temperature is guessed, based on which the mole fractions of all major species are calculated using their measured vibrational intensities. The mole fractions are then corrected using high-temperature correction factors to account for changes in the fraction of the Raman band falling in the exit slits provided for the respective photomultiplier tubes. The iteration process is repeated

until the sum of the mole fractions is unity; and (3) Rayleigh scattering: Raman data on the major species were used to obtain the Rayleigh cross section of the mixture and thus provide temperature in an iterative manner.

The last two methods agreed best, to within 10 K on mean temperature and to within 50 K on a shot-to-shot basis. Hence, method (2), based on the sum of mole fractions of major species, is reported below.

Initial measurements with the Raman system showed that there was significant laser-induced fluorescence (LIF) interference throughout the flame, as has also been reported elsewhere [15,16]. The LIF was fairly broadband and contaminated all Raman channels, but it was negligible in the Rayleigh channel. An additional difficulty encountered in the application of Raman to this flame was the cross talk between $CH_4$ and other Raman channels, primarily $O_2$. For the 488-nm excitation used here, the Raman interference in other major species was insignificant. To account for these two additional sources of contamination in the signals, the system and calibration procedures were modified. Additional PMTs were installed in two Raman-free regions of the spectra to monitor the LIF on a shot-to-shot basis. These PMTs, termed $F_1$ and $F_2$, were located at 540 nm (between $O_2$ and $CO_2$) and at 590 nm (between $CH_4$ and $H_2O$), respectively. These two signals were found to correlate very well with each other and with all other Raman signals so that the use of $F_1$ was found to be sufficient to allow corrections in all other channels.

A calibration procedure was used to correct for the LIF [15]. A 38-mm-diameter honeycomb burner was built to provide laminar diffusion flames of 30% $CH_4$/70% CO. The flame was visibly sooty and yellow at the downstream end and contained enough soot precursors and LIF at the upstream end to allow calibrations. The calibration factors were obtained by iteration. First, the raw data were used to calculate the temperature (from the sum of mole fractions) and mole fractions of major species. The contamination caused by fluorescence was particularly evident in the fuel-rich regions of the flame. The next step was to estimate correction factors for each of the major species based on the raw data and to subtract a term equal to the product of the correction factor for species $i$ and the value of the fluorescence signal measured in photomultiplier tube $F_1$. The calculated temperature and mole fraction profiles were then compared with the predicted values. The process was iterated to convergence. Figure 2 shows the temperature and selected species so obtained. The temperature agrees fairly well with the predicted laminar flamelet calculations [5] for an assumed stretch of 5/s; the calculations did not depend strongly on this assumed value. The corrections for $N_2$, $O_2$, and $CH_4$ are substantial, and the corrected species data again agreed with the laminar flame calculations, which are omitted for clarity. The calibration procedures were repeated before and after each set of measurements.

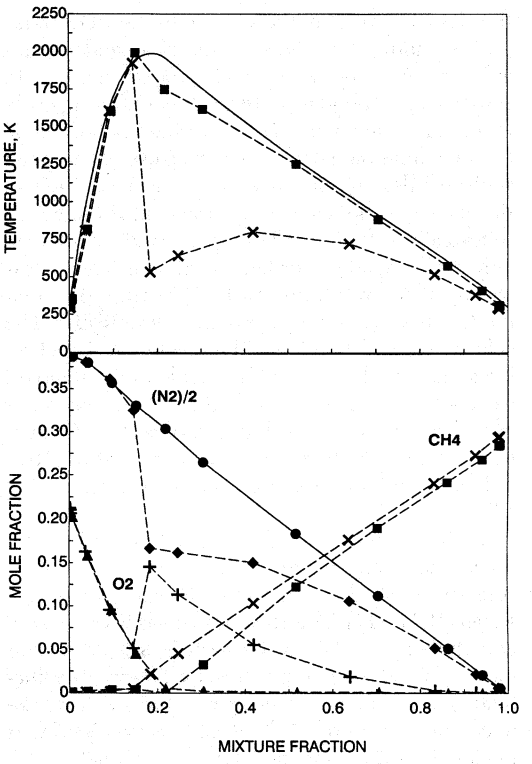


FIG. 2. Raw and fluorescence-corrected Raman data. Temperature: X = raw data; ■ = corrected data; solid line = laminar flame calculation from Ref. 5. Species (raw data): ◆ = $N_2$; + = $O_2$; and X = $CH_4$; corrected data: ● = $N_2$; ▲ = $O_2$; and ■ = $CH_4$.

Radial profiles of temperature and mole fractions of major species were measured at axial locations of $x/d$ = 5, 10, 20, 30, 50, and 70 and along the centerline. Since not all these data can be discussed here, attention will be confined to the region of maximum turbulence, $10 \leqq x/d \leqq 20$.

## Joint PDF/Elliptic Mean Flow CFD Model

To extend the PDF model from parabolic to elliptic flows, an iterative PDF/elliptic computational fluid dynamics (CFD) approach has been developed [9]. The highly nonuniform CFD grid accounts for the disparate flow scales imposed by the jet and bluff body dimensions, with enough resolution and with a second-order accurate numerical discretization scheme to eliminate numerical "diffusion" errors [3].

In the joint PDF model, the turbulent flow is described by the velocity $U$, the mixture fraction $\xi$, and

the reactive scalars in the system. In the PDF transport equation, these become the independent variables denoted by $V$, $\psi$, and $\phi_k (k = 1, \ldots, 4)$, respectively. The joint PDF evolves in this eight-dimensional velocity-composition space as well as in the two-dimensional $x$-$r$ physical space. A one-point statistical description in terms of the joint PDF of the velocity and these scalars is sought. If the flow is statistically stationary, all one-point statistics depend only on the spatial coordinates. All one-point statistics are recovered from this PDF because the composition is a known function of the above scalars. The velocity-composition joint PDF evolution model relaxes many of the assumptions made in the standard closure, such as PDF shape, statistical independence of scalars, and gradient diffusion of scalars. Closure of the nonlinear chemical source term and the "turbulent fluxes" of scalars are given directly by the PDF.

Turbulent mixing of the scalars is modeled as a linear, deterministic relaxation to the local mean, sometimes called Interaction-by-Exchange-with-the-Mean (IEM) [17]. The IEM model has been isolated and studied in detail in the partially stirred reactor model [12,18]. Regarding the velocity term, the fluctuating component of acceleration (arising from the fluctuating pressure gradient and viscous forces) is modeled by the simplified Langevin model [9,19]. The Seshadri–Peters, four-step reduced scheme is adopted for the kinetics [20]. A look-up table of reaction rates, density, and temperature is constructed on a nonuniform 20 × 10 × 10 × 10 × 10 grid.

The axisymmetric elliptic mean flow CFD model and the PDF model communicate with each other iteratively. Details are given in Ref. 9. On each time step, the fields of the mean velocity and the turbulence frequency, obtained from the local turbulence kinetic energy (TKE) and dissipation rate, are passed from the CFD model to the PDF model. A shift and a uniform stretching in $V$ space are applied to the PDF so that the mean velocity and the TKE of the two submodels are in agreement. Thus, the no-slip boundary condition is automatically satisfied at walls. Stochastic Lagrangian particle evolution, per the IEM model and the reduced scheme, occurs at the above frequency. The mean density field is passed back to the CFD model, and the two submodels are iterated to convergence. The 75 × 60 cell, $\approx 10^5$ particle calculation, was run until a statistical steady-state was achieved. For display purposes, lower moments such as the means were averaged over the last 200 time steps of the PDF evolution, reducing statistical fluctuations in the results. Scatterplots were prepared from the calculations by saving several realizations of the PDF particle array after stochastic convergence and then postprocessing the more than $10^6$ particles so obtained.

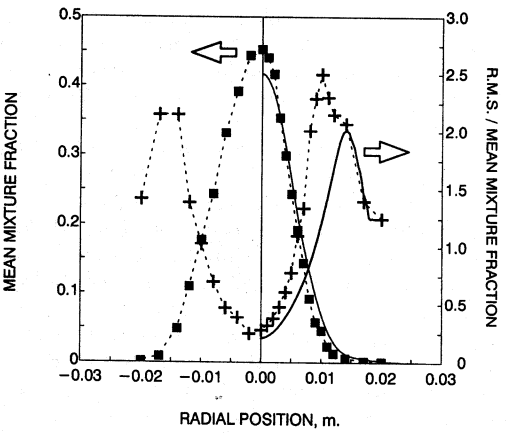


FIG. 3. Comparison of mean and rms mixture fraction profiles at $x/d = 20$. Raman data: ■ and +; Calculations: solid lines.

## Discussion

The following discussion focusses on the region of strongest turbulence ($10 \leqq x/d \leqq 20$), where the off-axis recirculation zone provides intense mixing at the edges of the jet.

Computed radial profiles of the mean and root mean square (rms) mixture fraction at $x/d = 20$ compare well with the Raman data (Fig. 3). The measured radial profiles are shown in full, revealing the degree of symmetry, while the computed profiles are by assumption axisymmetric. The comparisons indicate that the calculated mixture fraction field is accurate enough to permit a meaningful evaluation of the reactive quantities. The mean temperature peaks in the recirculation zone with a maximum of less than 1000 K, a result of the strong turbulence. Computations and data agree quite well (Fig. 4), although the temperature is underpredicted by almost 250 K along the centerline. The mean major species profiles also agree quite well (Fig. 5). The mean $O_2$ is depleted in the wake of the bluff body but coexists with mean $CH_4$, a consequence of finite-rate chemistry. The $O_2$ returns to ambient levels at the edge of the bluff body ($r \cong 0.02$ m). The model predicts more mean $O_2$ than measured at the centerline, which is consistent with underprediction of the mean temperature in Fig. 4.

Scatterplots provide an instructive format in which to study turbulence-chemistry interactions and best utilize the power of the time- and (not quite) space-resolved Raman spectroscopy and the PDF model. The measured temperature-mixture fraction scatterplot using all data from $x/d = 10$ and $x/d = 20$ is shown in Fig. 6a, along with the calculated laminar flame profile for a stretch of 5/s [5]. Unlike in the $CO/H_2$ flame [9], bimodality is clearly evident. A significant number of points has mixture fraction values

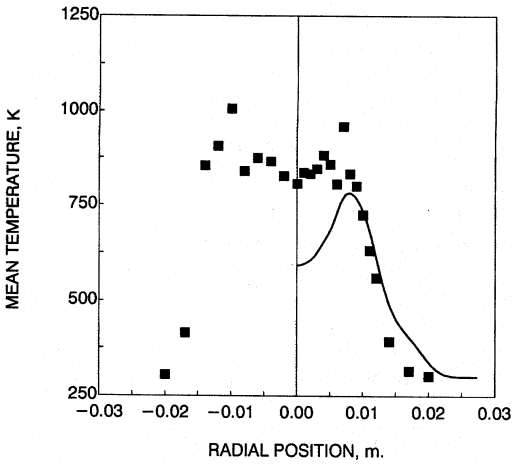


FIG. 4. Comparison of mean temperature profiles at $x/d = 20$.

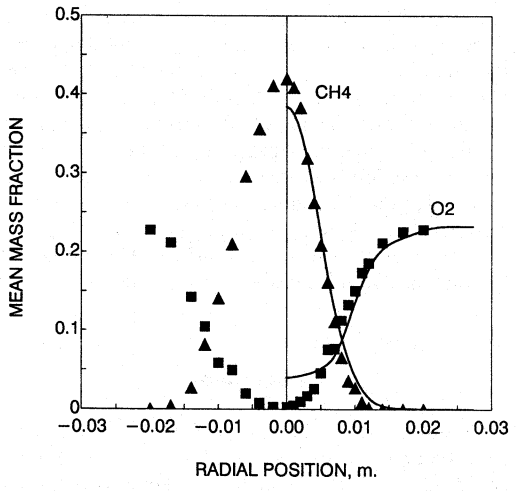


FIG. 5. Comparison of mean $CH_4$ and $O_2$ profiles at $x/d = 20$.

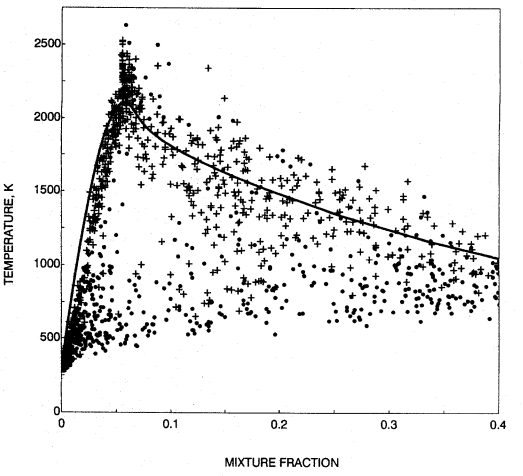


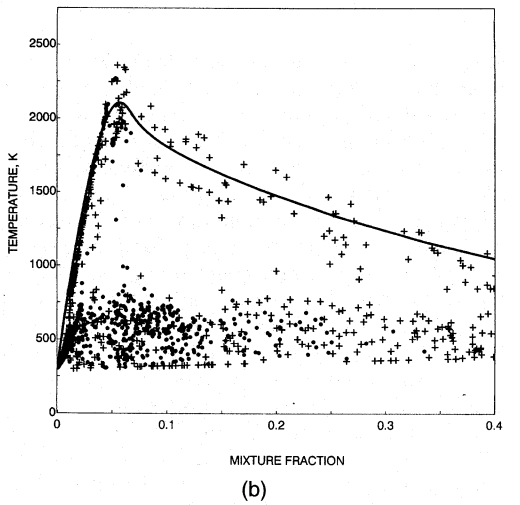


FIG. 6. Temperature-mixture fraction scatterplot at $x/d = 10$ (plus symbols) and $x/d = 20$ (solid symbols). Solid line is laminar flame calculation, from Ref. 5. (a) Raman data, (b) computed points.

close to stoichiometric but temperatures that manifest localized extinction, while other points are clustered along the line of strained flamelet temperatures. The physical picture that emerges from the scatterplots is that of a recirculation zone (which anchors the turbulent flame), connected to a jetlike region by a narrow neck of high shear with a significant amount of local extinction. The corresponding calculated scatterplot (Fig. 6b) is similar, although the predicted points exhibit a greater trend toward extinction. On a related note, stochastic calculations of lean methane-air combustion in a partially stirred reactor [12] showed that the parent starting scheme used to develop the four-step model agreed with a 77-step scheme reasonably well when the mean temperatures were above 1500 K but prematurely predicted blowout relative to the 77-step scheme. This behavior is similar to the overprediction toward extinction in the present study.

The coexistence of fuel and oxygen is again apparent in $Y_{CH_4}$-$Y_{O_2}$ scatterplots (not shown), from both the data and the model. The measured and calculated scatterpoints at $x/d = 20$, both of $T$-$\xi$ and $Y_{CH_4}$-$Y_{O_2}$, were closer to the chemically "frozen" line than those at $x/d = 10$, in accordance with Raman data and with visual observations of the flame.

The calculated CO scatterplots have maxima at 3% (inset, Fig. 7), whereas the data peak at about 10%

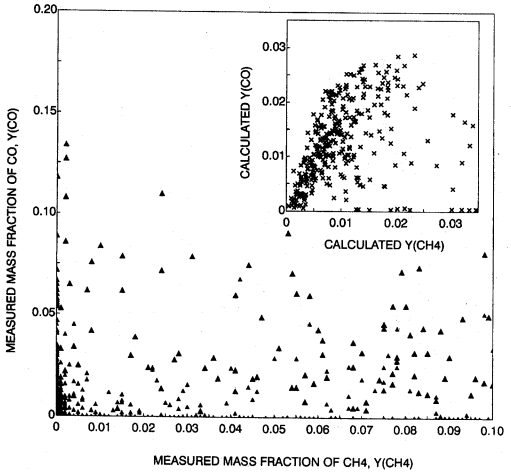


FIG. 7. CO-methane scatterplot at $x/d = 10$ and $x/d = 20$.

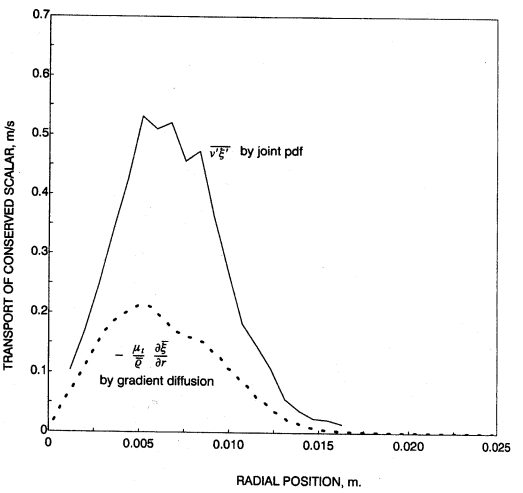


FIG. 8. Radial flux of conserved scalar at $x/d = 20$.

(Fig. 7), well above the flamelet maxima. Similar 10% levels were measured in Masri et al.'s bluff-body flame [13] and in pilot-stabilized flames [5], and 2–3% peaks were predicted in the latter using the four-step scheme within a (scalar) PDF/Reynolds stress model [5]. Hence, this discrepancy on CO maxima has appeared in diverse circumstances (but always in combustion gases that are near local extinction). There are many potential contributors, including (1) the assumption of a steady state for the radicals in the four-step mechanism; (2) the errors in Raman-based CO and $CO_2$ data, as discussed above and in Refs. 5 and 13 and as seen by direct comparison with predicted mean CO and $CO_2$ profiles in the $CO/H_2$ bluff-body flame of Ref. 9; and (3) neglection of phenomena such as unsteady flamelets or micromixed gases (perfectly stirred reactors) that have been shown to lead to high CO [21,22]. In intense turbulence, however, the microscale may be better simulated by the PaSR since it is the degenerate form of the PDF equation for spatially homogeneous systems. For example, at 30 atm, the PaSR indicates that approximately 2% peak CO levels are encountered until the fuel is pyrolyzed and CO oxidation can commence [23]. It seems clear that CO is an important clue to the microstructure of highly turbulent combusting gases and that accurate measurements will be critical.

The very large scatter about the conditional mean indicates that the CMC model [10] is inapplicable to this flow.

Because the joint PDF contains the velocity components of each particle, the scalar fluxes can be examined. Figure 8 shows the computed radial transport $\overline{v'\xi'}$ of the mixture fraction at $x/d = 20$, calculated by summing over particles in 20 radial bins. Also shown is the gradient diffusion flux $-(\mu_t/\bar{\rho})\,\partial\bar{\xi}/\partial r$, the latter computed from the mean fields; $\mu_t$ is the turbulent viscosity computed from the $k$-$\varepsilon$ equations. Both fluxes were calculated *a posteriori*, since they were not needed for the main computation. Figure 8 shows that in the presence of the strong radial gradient $\partial\bar{\xi}/\partial r$, (radial) transport of the mixture fraction is consistent with the notion of gradient diffusion; i.e., there is no countergradient diffusion. The magnitude of $\overline{v'\xi'}$ is, however, much greater than that of $-(\mu_t/\bar{\rho})\,\partial\bar{\xi}/\partial r$. The indicated "turbulent Schmidt number" is about 0.4.

## Conclusions

Complementary Raman measurements and joint PDF modeling have been used to study a turbulent nonpremixed methane-air flame stabilized behind a bluff body. The study demonstrates several points:

1. The bluff-body burner provides a strongly turbulent field leading to localized extinction, without the need for a pilot flame. Thus, the two-stream nature of the problem is preserved, unlike many piloted jet-flame studies where the composition or the excess enthalpy of the pilot flame can cause modeling difficulties. The present recirculation-stabilized flame is also much closer to practical burners.
2. By correcting for fluorescence, Raman measurements can be made in bluff-body $CH_4$-air flames; however, the errors in certain species (e.g., CO and $CO_2$) may be so large that models should not be changed on the basis of such data alone.
3. Given the similarity in scatterplots, it is clear that the *pointwise* structure of the above bluff-body flame and the piloted jet flame are quite similar,

in agreement with previous work. A greater degree of local extinction is measured here.

4. The limitations of PDF shape assumption, statistical independence of scalars, and gradient diffusion are removed from this "elliptic" model. The consequences of these can be seen in joint scatterplots and in convective fluxes.

The acquisition of Raman data and the three-velocity/five-scalar joint PDF calculation in this bluff-body methane flame takes each "discipline" to the limits of the present state of the art. Any significant further progress is likely to require improvements in major species measurements, complementary velocity and minor species measurements, and parallel computers. Reduced chemistry schemes that relax steady-state assumptions (and are likely to require additional scalars) will have to be developed and assessed in simpler contexts.

*Acknowledgment*

The work at GE is supported in part by the Air Force Office of Scientific Research, Contract No. F49620-91-C-0072, Dr. Julian Tishkoff, Project Manager.

REFERENCES

1. Bowman, C. T., *Twenty-Fourth Symposium (International) on Combustion*, The Combustion Institute, Pittsburgh, PA, 1992, pp. 859–878.
2. Correa, S. M., *Combust. Sci. Technol.* 87:329–362 (1992).
3. Correa, S. M., and Shyy, W., *Prog. Energy Combust. Sci.* 13:249–292 (1987).
4. Pope, S. B., *Twenty-Third Symposium (International) on Combustion*, The Combustion Institute, Pittsburgh, PA, 1990, pp. 591–612.
5. Chen, J.-Y., Kollmann, W., and Dibble, R. W., *Combust. Sci. Technol.* 64:315–346 (1989).
6. Correa, S. M., Gulati, A., and Pope, S. B., *Combust. Flame* 72:159–173 (1988).
7. Taing, S., Masri, A. R., and Pope, S. B., *Combust. Flame* 95:133–150 (1993).
8. Norris, A. T., and Pope, S. B., "Modeling of Extinction in Turbulent Diffusion Flames by the Velocity-Dissipation-Composition PDF Method," submitted to *Twenty-Fifth Symposium (International) on Combustion*, Irvine, CA, July 31–August 5, 1994.
9. Correa, S. M., and Pope, S. B., *Twenty-Fourth Symposium (International) on Combustion*, The Combustion Institute, Pittsburgh, PA, 1992, pp. 279–285.
10. Smith, N. S. A., Bilger, R. W., and Chen, J.-Y., *Twenty-Fourth Symposium (International) on Combustion*, The Combustion Institute, Pittsburgh, PA, 1992, pp. 263–269.
11. Chen, J.-Y., and Kollmann, W., *Twenty-Third Symposium (International) on Combustion*, The Combustion Institute, Pittsburgh, PA, 1990, pp. 751–757.
12. Correa, S. M., and Braaten, M. E., *Combust. Flame* 94:469–486 (1993).
13. Masri, A. R., Dibble, R. W., and Barlow, R. S., *Twenty-Fourth Symposium (International) on Combustion*, The Combustion Institute, Pittsburgh, PA, 1992, pp. 317–324.
14. Drake, M. C., Lapp, M., and Penney, C. M., "Use of Raman Effect for Gas-Temperature Measurement," in *Temperature, Its Measurement in Science and Industry*, (J. F. Schooley, Ed.), 1982, Vol. 5, p. 631.
15. Dibble, R. W., Starner, S. H., Masri, A. R., and Barlow, R. S., *Appl. Phys.* B51:1727–1731 (1990).
16. Masri, A. R., and Dibble, R. W., *Twenty-Second Symposium (International) on Combustion*, The Combustion Institute, Pittsburgh, PA, 1989, pp. 607–618.
17. Borghi, R., *Prog. Energy Combust. Sci.* 14:245–292 (1988).
18. Correa, S. M., *Combust. Flame* 93:41–60 (1993).
19. Pope, S. B., *Ann. Rev. Fluid Mech.* 26:23–63 (1994).
20. Seshadri, K., and Peters, N., *Combust. Flame* 81:96–118 (1990).
21. Mauss, F., Keller, D., and Peters, N., *Twenty-Third Symposium (International) on Combustion*, The Combustion Institute, Pittsburgh, PA, 1990, pp. 693–698.
22. Chen, J.-Y., and Dibble, R. W., *Combust. Sci. Technol.* 84:45–50 (1991).
23. Correa, S. M., "Models for High-Intensity Turbulent Combustion," *Comp. Sys. Eng.* 5 (2):135–145 (1994).